

PhD Thesis (extract):
Multi-Scale Modeling and Variability
in Cardiac Cellular Electrophysiology

Michael Peter Éamon Clerx

April 24th, 2017

CHAPTER 2

Background: Bioelectricity in the human heart

Abstract

This chapter provides some of the biological and modeling background needed to read this thesis. References to more detailed works are given throughout the text.

The heart uses bioelectrical signals called *action potentials* (APs) to coordinate its contraction. These signals originate at the cellular level, and are caused by the movement of charged particles (ions) through channels and transporters in the cell membrane. Action potentials propagate from cell to cell, creating traveling waves of excitation that trigger contraction of the heart muscle. The aggregate electrical currents through the billions of muscle cells in the human heart give rise to a signal powerful enough to be measured on the body surface: the electrocardiogram or ECG.

Using modern measurement techniques and novel pharmacological compounds, it has become possible to study the ionic currents through several distinct ion channels and transporters. Each of these currents can be described using numerical models, and models of currents can be combined into models of the cardiac cellular AP. These models describe the complex interplay between the currents and can even capture subcellular processes, including the release of Ca^{2+} which triggers the cell's contraction. Models of the single-cell AP can be combined into models of coupled cells, of patches of tissue and ultimately of the electrical system of the whole heart.

Contents

2.1	Bioelectricity in the human heart	4
2.2	The cellular action potential	5
2.3	Modeling the action potential	6
2.4	Modeling ionic currents	7
2.4.1	Hodgkin-Huxley models of ionic currents	8
2.4.2	A note about identifiability	10
2.4.3	Markov models of ionic currents	10
2.4.4	Single-channel simulations	11
2.5	Measuring currents and mutations	12
2.6	Modern AP models	14
2.7	The human ventricular epicardial AP	15
2.8	Models of coupled cells and tissue	17
2.9	Conduction velocity and reentry	17
2.10	Bioelectricity on the body surface	18
2.11	A personal note	19

2.1 Bioelectricity in the human heart

For all its complexity, the heart functions as a two-sided pump. Its right side pumps blood into the lungs to be oxygenated (the *pulmonary* circulation), after which it returns to the left side of the heart which pumps it to the rest of the body (the *systemic* circulation). Each side has an *atrium*, which functions as a receiving chamber and a preloading pump for the larger *ventricle*, which performs the main pumping action. The heart's capacity to pump efficiently comes from its ability to perform coordinated contractions: First, both the left and right atrium (LA and RA) contract, filling the left and right ventricles (LV and RV). Next, the ventricles contract, sending blood into the aorta (from the LV) and pulmonary artery (from the RV). A schematic overview is given in [Fig. 2.1.A](#).

This timed sequence of contractions arises from the individual contraction of each of the heart's muscle cells, which are known as *cardiac myocytes*. As the heart contains around five billion of these cells ([Olivetti et al., 1995](#)) this requires a high degree of synchronization. This is achieved through the use of *bioelectricity*. Like neurons, myocytes have evolved to sustain a brief electrical pulse and pass it on to their neighbors, causing the spread of an electrical signal in a 'Mexican wave' style ([Welsh et al., 2017](#)). This propagating cellular electrical signal is known as an *action potential*¹ (AP).

In addition, the heart contains smaller numbers of cells with specialized electrical functions: the cells of the *sinoatrial* (SA) node show spontaneous excitation (i.e., they spontaneously generate APs). This occurs about once per second, although this rate is regulated by different mechanisms in response to varying energy demand. In healthy conditions, the SA node sets the pace for the rest of the heart. From the SA node's location at the top of the right atrium, its electrical waves spread over the right and left atria through cell-to-cell conduction. This electrical excitation triggers contraction of the atrial muscle cells via *excitation-contraction coupling* ([Bers, 2001](#)).

The atria are electrically shielded from the ventricles, causing the propagating AP to halt at the atrial borders. Activation of the ventricles occurs via a second group of specialized cells which together form the *atrioventricular* (AV) node. Signals from the SA node reach the AV node, where they are slightly delayed while the atria contract and fill the ventricles. Next, the signals travel down conducting *Purkinje fibers* in the septum (the muscle wall which separates the LV and RV) towards the tip (or *apex*) of the heart. From there, they spread over the ventricular walls causing both ventricles to contract and perform a powerful pumping motion. A schematic overview of the heart's electrical conduction system is given in [Fig. 2.1.B](#).

¹ Readers with a background in physics may wish to note that it is not a potential in the physical sense of the word, i.e., it is not a measure of energy or electrical potential but simply the name given to a short electrical event.

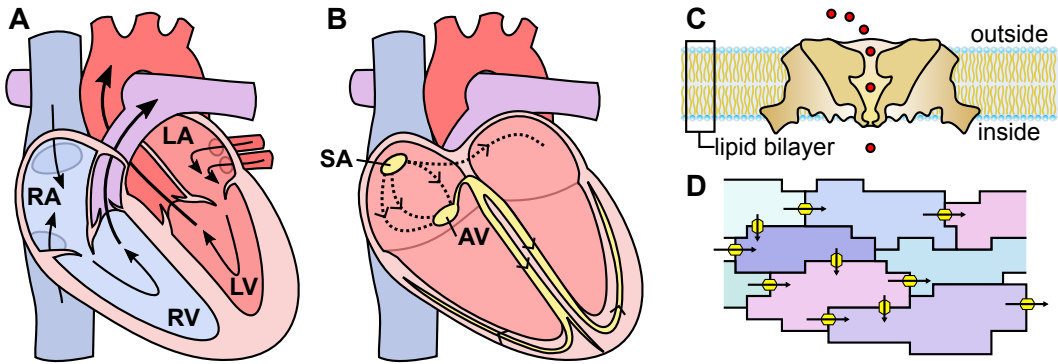


Figure 2.1: (A) Basic anatomy of the heart. Oxygen-depleted blood enters the right atrium (RA), is transported to the right ventricle (RV) and then pumped to the lungs. From the lungs, oxygen-rich blood enters the left atrium (LA) and then the left ventricle (LV) from where it is pumped into the aorta and then to the body. (B) A schematic overview of the heart's conduction system. Excitation starts at the sinoatrial node (SA) and travels over the atria before being propagated to the atrioventricular node (AV), where it is slightly delayed before being propagated to the ventricles. (C) A cross-section of a cell membrane, containing an ion channel. The shape of the channel is based on [Payandeh et al. \(2011\)](#). (D) A network of myocytes, connected by gap junctions.

2.2 The cellular action potential

How can cells conduct electrical waves? The answer depends crucially on the *cell membrane*, a thin water-insoluble layer that separates a cell's interior from its environment. The membrane is composed of phospholipids that have a polar (and hence hydrophilic) head and a non-polar (hydrophobic) tail. This property causes them to organize into a *lipid bilayer*, with heads pointing out and tails pointing in towards the center of the membrane (see [Fig. 2.1.C](#)). The non-polar core acts a strong electrical *insulator*, blocking the passage of any polar or charged particles, including naturally present ions such as sodium (Na^+), potassium (K^+) and calcium (Ca^{2+}). As a result, a cell can contain different concentrations of ions than the fluid outside it, allowing a difference in the density of electrical charge to arise. This charge imbalance can be expressed as an electrical potential difference called the *membrane potential*. Membrane potentials can be measured, and are usually in the order of tens of millivolts (about -100 to $+50\text{mV}$ in a cardiac cell). When ions move in or out of the cell, the membrane potential changes, producing the so called action potential.

Wedged into the cell membrane of cardiac myocytes are several proteins, some of which have remarkable properties. *Ion channels* are large macromolecular complexes that, under certain conditions, can 'open' to form an aqueous pore that allows ions to pass through the membrane. Most ion channels are highly selective, and include a narrow funnel-like structure whose electrochemical properties are such that only a single species of ion can pass through. The direction of movement depends on the ion's concentration gradient and the membrane potential. Some channels open and close only after binding to certain chemicals, but this thesis deals exclusively with ion channels that open and close in a *voltage-dependent* manner.

A cartoon of an ion channel inside a cell membrane is shown in [Fig. 2.1.C](#).

In addition to ion channels, the membrane contains so-called *pumps* that transport ions from one side of the membrane to the other. Pumps move ions *against* their chemical and/or electrical gradient, and the energy required to do so is obtained by breaking down ATP (adenosine triphosphate) into ADP (adenosine diphosphate). Similarly, *co-transporters* and *exchangers* move ions against their gradient, but they derive their energy from the simultaneous movement of a second type of ion, *along* its gradient. Pumps, exchangers and co-transporters are collectively known as *transporters* ([Molleman, 2003](#)).

Finally, myocytes are connected to their neighbors via special channels known as *gap junctions*. These form large, non-specific pores that allow strong ionic currents to pass between cells. Although gap junctions are weakly voltage sensitive, it is usually adequate to think of them as continuously open channels ([Gros and Jongsma, 1996](#)). Myocytes are around $140\mu\text{m}$ long and $25\mu\text{m}$ wide ([Volders et al., 1998](#)) and are usually arranged in a grid with similarly oriented cells. Most connections are at the short end of the cells, leading to faster AP propagation along the longitudinal axis of the fibers. A group of myocytes connected by gap junctions is shown schematically in [Fig. 2.1.D](#).

2.3 Modeling the action potential

In a groundbreaking series of papers published in 1952, Alan Hodgkin and Andrew Huxley presented the first *computational model* of a cellular AP ([Hodgkin and Huxley, 1952a,b,c,d](#)). By carefully measuring the different currents passing through the membrane of a squid axon, they were able to create models for the three main components of the axon's AP: a current carried by Na^+ , one carried by K^+ , and a 'leakage' current carried by anything else. They found that the size and shape of each current is strongly dependent on the membrane potential. As the membrane potential is a direct result of the ionic concentrations in and outside the cell, it changes when ions move across the membrane. This creates a feedback loop, shown in [Fig. 2.2](#) (left), where the membrane potential determines the transmembrane currents and the transmembrane currents determine the membrane potential. As a result, the process is best described as a *dynamical system*.

In computational models of the AP, variables are defined that represent the membrane potential, intracellular ion concentrations, and the state of all ion channels and transporters. Next, differential equations are defined that, given the model state at some time t , provide the derivatives of all variables. In other words, given the current state of the cell, they specify how it will *change*. This knowledge can then be used to make a prediction for the state of the model at time $t + \Delta t$, and by doing this repeatedly (with very small time steps Δt) simulations can be run (for a detailed overview of this and similar methods, see any book on *numerical integration of ordinary differential equations*).

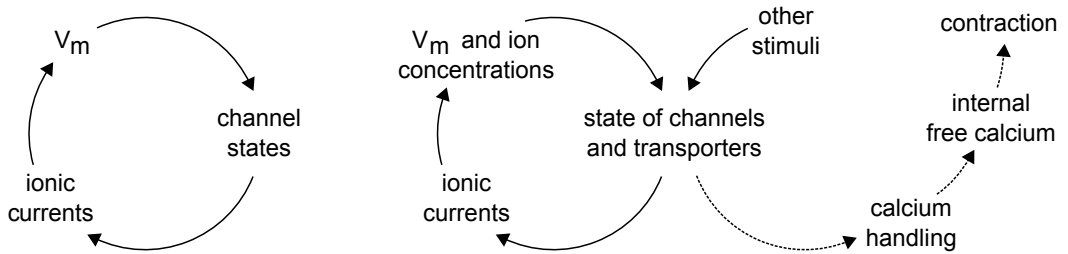


Figure 2.2: A classic (left) and updated (right) view of the feedback loop underlying models of the cellular action potential. In the classic view, the membrane potential V_m determines the channel states, which determine the ion currents through the membrane. The sum of the ionic transmembrane currents then determines the change in the membrane potential. To the right, an updated view is given where not only changes to V_m are modeled, but additional work is done to keep track of ionic concentrations in crucial parts of the cell. Ion channels, pumps, exchangers and even diffusion currents are modeled, all of which can be affected by stimuli from outside the cell. Particular attention is paid to the processes that determine the free Ca^{2+} concentration in the cell, which ultimately leads to contraction. Adapted from [Hille \(2001\)](#).

To give all this a mathematical representation, we define the membrane potential V_m as

$$V_m = V_{\text{in}} - V_{\text{out}}$$

where V_{in} and V_{out} are the electrical potentials inside and outside the cell respectively. Next, we define a *positive* current, as one that carries charge *out of the cell* (thus lowering V_{in} , raising V_{out} and decreasing V_m). The change this causes to the membrane potential is captured by the equation

$$\frac{dV_m}{dt} = -\frac{1}{C_m} I$$

where C_m is the membrane capacitance and I is the sum of all transmembrane currents. In Hodgkin and Huxley's model, this results in

$$\frac{dV_m}{dt} = -\frac{1}{C_m} [I_{\text{Na}} + I_{\text{K}} + I_{\text{leak}}].$$

Here, I_{Na} , I_{K} and I_{leak} represent the sodium, potassium and leak current respectively. Later models added new currents and refined the existing ones, leading to a more complicated equation but following the same general form (see Chapter ??). A detailed introduction to AP modeling can be found in [Rudy and Silva \(2006\)](#). The next step is to model the ionic currents, which is discussed in the following section.

2.4 Modeling ionic currents

Models of ionic currents start from Ohm's law $I = \Delta V/R$, where I is the current, R is an electrical resistance and ΔV is a difference in electric potential. Instead of using resistance, current modelers use *conductance* $G = 1/R$, with the S.I. unit *siemens* or *S*. The appropriate voltage difference ΔV is determined by a combination of electrical forces and *diffusion*:

When channels are open, ions can diffuse from the side with the higher concentration to the side with the lower. But since ions are charged they are also affected by the presence of any electrical field. Thus, ion currents depend on chemical as well as electrical gradients. Currents will flow until these two forces reach equilibrium at a potential E , known as the *Nernst* or *equilibrium* potential. In other words, they will flow until $\Delta V = V_m - E = 0$.

For convenience, a changing conductance is usually written as the product of a dimensionless time-variant term $g(V_m(t), t)$ and a fixed factor \bar{g} that can be used to scale the current, for example to model different cell sizes, changes in the number of channels (due to regulation of genetic expression) or drug-induced block. This results in a general equation of the form

$$I = \bar{g} \cdot g \cdot (V_m - E)$$

There are two main formalisms used to model the variable conductance term g : *Hodgkin-Huxley style models* and *Markov models*. Both will be discussed below. For a major reference work on ion channels and ion channel models, see [Hille \(2001\)](#).

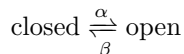
2.4.1 Hodgkin-Huxley models of ionic currents

The current models introduced by Hodgkin and Huxley (HH) describe the conductance term g as the product of one or more dimensionless variables, whose value can vary between 0 and 1. Each variable can appear in the product once or multiple times (i.e., some variables are raised to an integer power). For example, for the sodium current I_{Na} , HH introduced the variables m and h , with m appearing three times, to obtain:

$$I_{\text{Na}} = \bar{g}_{\text{Na}} \cdot m^3 \cdot h \cdot (V_m - E_{\text{Na}})$$

where E_{Na} is the reversal potential for Na^+ , which depends on the Na^+ concentrations in and outside the cell. Intuitively, the term $m^3 \cdot h$ can be thought of as a series of three synchronized m -type gates, followed by a single h -type gate, where the m and h -type gates open and close independently of each other. The variables m and h then represent the proportion of gates in the membrane that are in the open state. If all gates are open ($m = h = 1$) the current is at its peak, but no current can flow if either m or h is zero.

Opening and closing of a gate is modeled as a chemical reaction:



where α and β are the opening and closing rates (in units 1/second). We can then write an equation that shows how a proportion such as m changes over time (we use m in the example, but equations of the same form are used for h or any other gating variable):

$$\frac{dm}{dt} = \alpha_m(1 - m) - \beta_m m$$

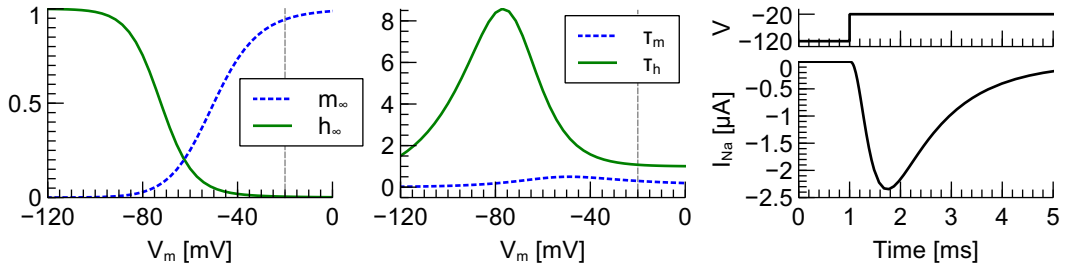


Figure 2.3: The steady states (left) and time constants (center) for gating variables m and h , calculated from the equations for the sodium current given in (Hodgkin and Huxley, 1952d). The current elicited by a voltage step from -120 mV to -20 mV is shown on the right. Before the voltage step ($t < 1$) a low membrane potential $V_m = -120$ mV is maintained. At this voltage, the model is not activated ($m = 0$) and completely recovered from inactivation ($h = 1$), as can be seen in the left panel. At $t = 1$ ms, the potential is quickly raised to -20 mV causing the model to activate ($m \rightarrow 1$) with a speed dictated by τ_m . It also immediately starts inactivating ($h \rightarrow 0$) but this happens at a lower speed than activation (center panel), leading to the temporary appearance of an ionic current (lower right panel). After a few milliseconds at -20 mV, the model is fully activated ($m = 1$) but also fully inactivated ($h = 0$) so that a current can no longer be observed.

This is often rewritten in the form $dm/dt = (m_\infty - m)/\tau_m$ with $m_\infty = \alpha_m/(\alpha_m + \beta_m)$ and $\tau_m = 1/(\alpha_m + \beta_m)$. With this formulation, it can be seen that every gate variable (in this case m) approaches a steady state value (m_∞) with a speed determined by some time constant (τ_m). The steady state and time constant are taken to be the voltage dependent parts of the system, so that

$$\frac{dm}{dt} = \frac{m_\infty(V_m) - m}{\tau_m(V_m)}$$

The process of fitting a HH-style model to a current, then, is the process of: 1. Postulating the number of gate types (typically using the smallest number that can fit the observed data). 2. Measuring the steady states and time constants for a range of values of V_m . 3. Choosing equations to fit this data and finding the parameters that give the best match. 4. Tweaking the result by adding powers to the gating variables (again, using the smallest power that gives an adequate fit).

The steady state and time constant curves obtained by HH for the sodium current in the squid axon are shown in Fig. 2.3. These curves were highly influential for the methodology and terminology of cellular electrophysiology. The variable m became known as an *activation* variable, with the transition from $m = 0$ to $m = 1$ known as activation and the reverse process sometimes known as deactivation. Similarly, the decrease in h seen at higher potentials is now known as *inactivation*, while its transition back to 1 is called recovery from inactivation, or simply recovery. The potential at which $m_\infty = 0.5$ is known as the *midpoint of activation* and the point at which $h_\infty = 0.5$ is the *midpoint of inactivation*. These terms have stuck, and are often used outside the context of modeling or even when discussing competing current model formalisms.

2.4.2 A note about identifiability

The steady states and time constants of HH-style models cannot be measured directly, but must be inferred from recordings of the current. This raises concerns about the model's *identifiability*, i.e., the possibility of finding the ‘true’ model parameters based on recordings of I . In their analysis, Hodgkin and Huxley relied on the crucial assumption that the time constant of m is much smaller than that of h , causing m to change much faster. The difference in speed allows the start of a recording to be used to estimate the parameters for m , while the end can be used to estimate the parameters of h . This is discussed further in Chapter ??.

2.4.3 Markov models of ionic currents

When Hodgkin and Huxley created their model of currents and the AP, the mechanism by which ions moved through the membrane was still unknown. Later, as the recognition of ion channels grew, models emerged that attempted to describe changes in channel protein conformation as a means of predicting currents. These became known as *Markov models*².

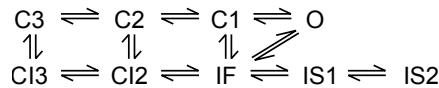


Figure 2.4: A Markov model structure for I_{Na} introduced by Clancy and Rudy (2002).

An example of a Markov model structure for the cardiac sodium current is shown in Fig. 2.4. It defines 9 states, one of which is the open state (O). In addition, there are three closed states (C3, C2, C1), two closed-inactivated states (CI3 and CI2), a ‘fast’ inactivated state (IF) and two ‘slow’ inactivated states (IS1 and IS2). Like in the HH formalism, transitions between states are governed by voltage-dependent chemical reaction rates. Using this model, the sodium current through a cell membrane is modeled as:

$$I_{Na} = \bar{g}_{Na} \cdot O(V_m) \cdot (V_m - E_{Na})$$

where $O(V_m)$ is the proportion of channels in the open state.

This model shares similarities with the I_{Na} model introduced by Hodgkin and Huxley. To activate, the model makes three jumps ($C3 \rightarrow C2 \rightarrow C1 \rightarrow O$) after which inactivation can set in ($O \rightarrow IF$). It is also possible for the model to be deactivated ($m = 0$) and inactivated ($h = 0$) at the same time (CI3 and CI2). However, the Markov model structure allows for the introduction of dependencies between state transitions: the inactivated states IS1 and IS2 can only be reached via the state IF. These states were introduced to represent an

²Readers familiar with statistical Markov chains should note that the models used in cell electrophysiology use chemical reaction rates instead of transition probabilities, leading to slightly different mathematics.

experimentally observed slow inactivation process, where channels that were kept at high potentials for an extended period needed a long time to recover (Clancy and Rudy, 2002).

Markov models have long been investigated as a way to connect ion-channel characteristics to measurable currents (Armstrong and Bezanilla, 1977). This has been successfully used to extrapolate from changes in single-channel function to clinically relevant changes in the AP (Clancy and Rudy, 1999). Conversely, it can be used to learn about channel properties (for example state-dependent effects of channel-blocking drugs) by inspecting differences in measured currents (Clancy et al., 2007).

If a channel's kinetics can be well described as discrete transitions between a limited number of states, and if we can identify those states, write down equations and parametrize the resulting model, then Markov models present a unique bridge between molecular-level effects and whole-cell currents. However, like the problem of finding the number of gates and the powers in HH-style models, the problem of determining the structure of a Markov model is still unsolved, although good estimates can be made by combining different sources of information (Armstrong, 2006). Similarly, the shape of the equations that describe the rate constants is chosen freely by the modeler (but equations based on *Eyring rate-theory* have also been used, see Irvine et al., 1999). Finally, simulations with Markov models are slower than those using HH-style models, especially when tricks are used to reduce the run-time (see Rush and Larsen, 1978, and Chapter ??). For a recent overview of the differences between HH-style and Markov models, see Carbonell-Pascual et al. (2016).

2.4.4 Single-channel simulations

The discovery of ion channels allowed Hodgkin and Huxley's ion current models to be interpreted as descriptions of the current carried through the membrane by *all* channels of a certain type. When the current through *individual* channels was measured in the 70s (see Section 2.5) it confirmed earlier suspicions³ that they opened and closed stochastically, with opening and closing probabilities dictated by the membrane potential. By selecting the appropriate algorithm, Markov models can be used to simulate both the stochastic single-channel currents (Gillespie, 1976) and the idealized aggregate current through large numbers of channels.

Fig. 2.5 shows the stochastic opening and closing of cardiac sodium channels, simulated with the model by Clancy and Rudy (2002) (using *Myokit*, see Chapter ??). According to this model, channel openings are relatively rare events, even at potentials leading to strong aggregate currents. As the number of channels increases, the probability of multiple channels being open at the same time increases. For larger numbers of channels, the sum of the stochastic openings increasingly resembles the idealized aggregate current.

³ In fact, good estimates of the number of channels and their individual conductances had already been made using statistical models, see for example Hille (1970) or Katz and Miledi (1972).

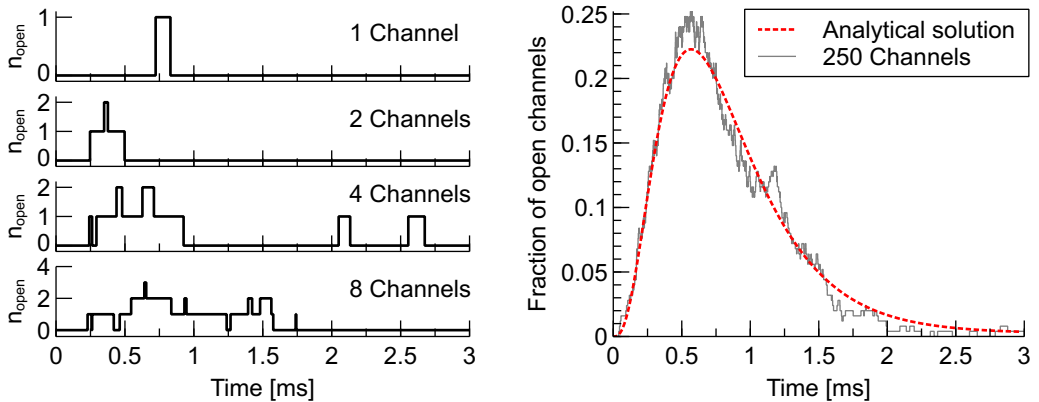


Figure 2.5: Stochastic sodium channel openings, simulated using the model by [Clancy and Rudy \(2002\)](#) for a single voltage step from -120mV to -20mV . (*Left*) The total number of open channels, simulated in a model with 1, 2, 4 or 8 channels. (*Right*) The fraction of open channels in a stochastic simulation with 250 channels (noisy line) and the idealized aggregate curve (smooth line).

2.5 Measuring currents and mutations

The first (indirect) recording of an AP occurred as early as 1868, when the German physiologist Julius Bernstein invented the “differential rheotome” and used it to measure impulse propagation in frog nerve ([Schuetze, 1983](#)). He hypothesized that his findings could be explained if cells had an electrically isolating membrane, occasionally permeable to potassium ions ([Seyfarth, 2006](#)). Direct recording of ionic currents became possible in 1947, when George Marmont and Kenneth S. Cole realized that a feedback amplifier could be used to control the membrane potential while simultaneously measuring transmembrane currents⁴. In their early experiments they used the giant axon of the squid *Loligo pealeii* (now known as *Doryteuthis pealeii*), an unusual cell type which had the advantage of being large enough to allow the insertion of a metal electrode directly into the axon. This technique of controlling the membrane potential with a feedback amplifier became known as *voltage clamping* ([Cole, 1968](#); [Huxley, 2002](#); [Verkhatsky et al., 2006](#)).

Later, voltage clamping was applied to other cell types by using glass *micropipettes* (with a very sharp tip) to penetrate the cell membrane. Provided the pipette tip is small enough for the membrane to survive the perforation, an electrical connection with the cell interior can be made by filling the pipette with a buffered salt solution and inserting an electrode into its wider end ([Graham and Gerard, 1946](#)). Combined with voltage-clamp, this technique can be used to measure APs and transmembrane currents (see also [Hodgkin, 1950](#)) and in 1949 the first micropipette measurements of the cardiac AP were reported by [Coraboeuf and Weidmann \(1949\)](#).

⁴ Guitar players might be interested to learn that, while the transistor had been developed in the very same year, the first voltage-clamp amplifiers were in fact tube amplifiers.

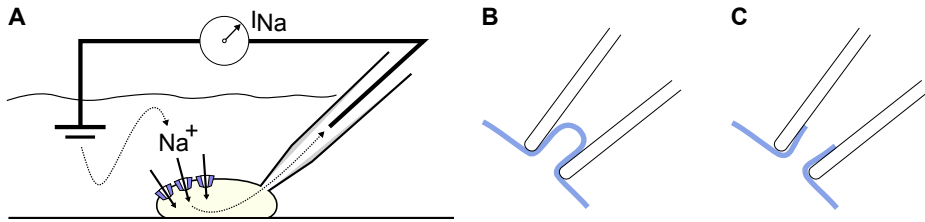


Figure 2.6: (A) A schematic overview of the whole-cell patch-clamp configuration. (B) Pipette attached to a cell. Some suction is applied, causing the membrane to enter the pipette and form a tight seal. (C) After applying another short burst of suction, the membrane ruptures but stays attached to the inside of the pipette.

In 1976, Neher and Sakmann discovered they could use a pipette with a larger tip (a *low-resistance electrode*) to electrically isolate a small patch of membrane, allowing the recording of currents through a single channel (Neher and Sakmann, 1976). Different variations on this concept appeared in the years following their discovery, which collectively became known as *patch clamping*. A popular method, employed in Chapter ??, is the ‘whole-cell configuration’ which measures aggregate whole-cell currents instead of single-channel currents. In this set-up, shown schematically in Fig. 2.6.A, a pipette is placed *against* the cell membrane (using a microscope and a mechanical micro-manipulator on a stabilized table). Some suction is then applied, causing a small patch of tissue to enter the pipette and form a tight seal (Fig. 2.6.B). Once the seal has stabilized, a second short burst of suction (or ‘kiss’) is applied that, if successful, ruptures the membrane but leaves it attached to the inside of the pipette, allowing electrical access to the cell interior (Fig. 2.6.C).

The next big advance occurred when genes encoding ion-channel subunits were identified and cloned. In 1984, Noda et al. were able to transcribe the DNA sequence for the sodium channel of the electric eel *Electrophorus electricus* (Noda et al., 1984). Electric eels were the ideal candidate as their *electroplax* (the electric organ used to shock prey with) contains a very high density of sodium channels. Two years later they artificially inserted this DNA into *Xenopus* oocytes (frog eggs), and managed to record currents from the ion channels then expressed by these cells (Noda et al., 1986).

The technique of inserting cloned channel DNA into such an *expression system* was further developed to allow the study of *artificially mutated genes*. This has had a great impact on medicine, as it allows mutations in channel genes identified in a clinical setting to be recreated and studied in the laboratory. In Chapter ?? we use measurements in cell-expression systems to investigate the possibility of variability in the kinetics of I_{Na} . In Chapter ?? we analyze a large number of patch-clamp experiments on mutated sodium channels in expression systems, and attempt to predict how the mutations affect the ionic current.

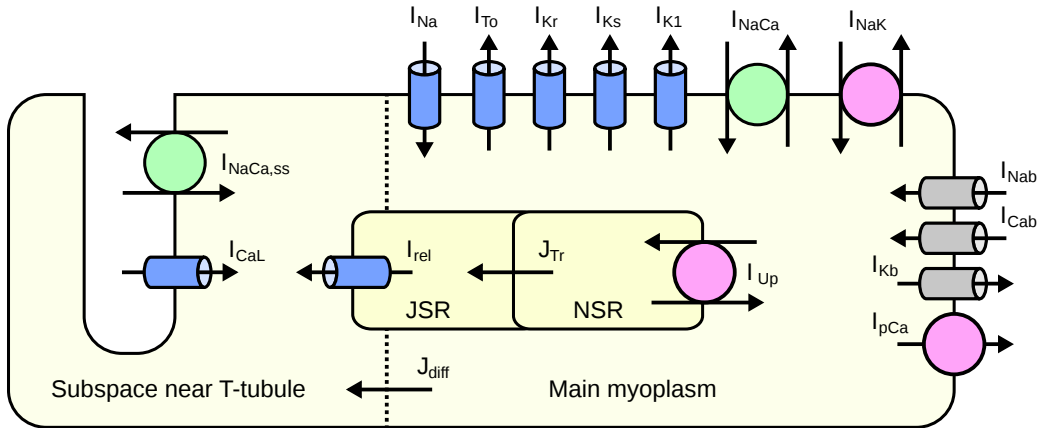


Figure 2.7: Simplified schematic of a model of the ventricular action potential (O’Hara et al., 2011). The cell is split into the main myoplasm, the area near the t-tubules and two compartments relating to Ca^{2+} storage and release (the JSR and NSR, see text). Channels are shown in blue, pumps in red and exchangers in green. Background currents are indicated as gray channels.

2.6 Modern AP models

In 1962, ten years after Hodgkin & Huxley’s model of the squid axon, the first computational model of a cardiac cell was developed by Denis Noble (1962). This model described the AP of cells from the Purkinje fibers. Like the HH model, it used just three currents (sodium, potassium and leak) and made no predictions about ion concentrations in the cell. In 1977, a model of the (mammalian) ventricular AP was introduced by Beeler and Reuter (1977), which included a Ca^{2+} current and a method for tracking the internal Ca^{2+} concentration. The model also split the potassium current into two distinct components. This trend of tracking concentrations and adding or refining currents continued in the next decades, causing models to grow larger and ever more specific. ‘Mammalian’ models were replaced with species-specific ones (dog, rabbit, mouse, human, etc.) and different models were created for cells from the SA node, the atria, Purkinje fibers, the LV and RV, and even for cells from the outer (*epicardial*) or inner (*endocardial*) layer of the LV. For a detailed overview, see Noble et al. (2012).

Fig. 2.7 shows a schematic overview of a modern model of the ventricular epicardial AP (O’Hara et al., 2011). It includes a fast sodium current (I_{Na}) and a three-part leak (or background) current ($I_{\text{Nab}} + I_{\text{Cab}} + I_{\text{Kb}}$). The potassium current has been split into four different parts, each through a different channel type with its own distinctive characteristics. In addition, a Ca^{2+} current (called I_{CaL}) has been introduced, along with several pumps and exchangers.

The cell interior is divided into several compartments, and the model tracks ionic concen-

trations (particularly Ca^{2+}) in each of these, as well as the diffusion between them. The *network* and *junctional sarcoplasmic reticulum* (NSR and JSR) are structures inside the cell that play a crucial role in *Ca^{2+} -induced Ca^{2+} release*, a process whereby the entry of a small amount of Ca^{2+} through the membrane triggers the release of large amounts of Ca^{2+} from the sarcoplasmic reticulum (Bers, 2001). Ventricular myocytes are known to have an extensive network of *t-tubules*; places where the membrane folds inwards to create deep “invaginations” that bring the sarcoplasmic reticulum into close proximity with the extracellular fluid (see Soeller and Cannell, 1999, for 3-dimensional images of the t-tubular network). In the model shown here, the area near the t-tubules is modeled as distinct from the bulk intracellular fluid (or *myoplasm*). These detailed channels, transporters and compartments are crucial in modeling the complex processes of excitation-contraction coupling that lead to contraction of the muscle cell. An updated version of the cyclic interaction between membrane potential, channel states and currents is shown in Fig. 2.2 (right).

The development of complex models such as these has led to the need for tools that simplify model implementation, exchange, and comparison. In Chapter ??, *Myokit* is introduced as a toolkit for development and rapid simulation of modern models of the AP. For a comparison of the complexity of modern models, see Heijman (2012).

2.7 The human ventricular epicardial AP

One of the advantages of computational modeling is the ability to simulate and visualize the complex interaction between model components. Fig. 2.8 shows how currents in the model by O’Hara et al. (2011) act together to shape the human ventricular epicardial AP. For the sake of simplicity, some of the smaller currents are omitted, and no details of the internal currents and diffusion are shown. While model- and cell-specific, the main components for this model are similar to those in many cardiac myocytes, and will be discussed below as a general introduction to the different currents and their role in shaping the AP.

At the start of the simulation shown in Fig. 2.8, the cell is fully relaxed (not contracted) and V_m is at a stable *resting potential* of around -88mV . After 30ms, a short pulse is applied to the cell (i.e., a small inward current is injected). This raises the membrane potential just enough for the sodium current I_{Na} to activate, triggering a significant rise in the membrane potential. As the sodium current begins to inactivate, the increase in membrane potential slows down, eventually leading to a peak of around 35mV . At this high potential, the transient outward potassium current I_{To} activates and then rapidly inactivates, causing a small notch in the AP that is characteristic for epicardial ventricular cells. The next currents to activate are the L-type calcium current I_{CaL} and the rapid delayed rectifier potassium current I_{Kr} . These currents act in opposing directions, causing the membrane potential to stay relatively stable for a period of about 200ms known as the *plateau phase*. During the

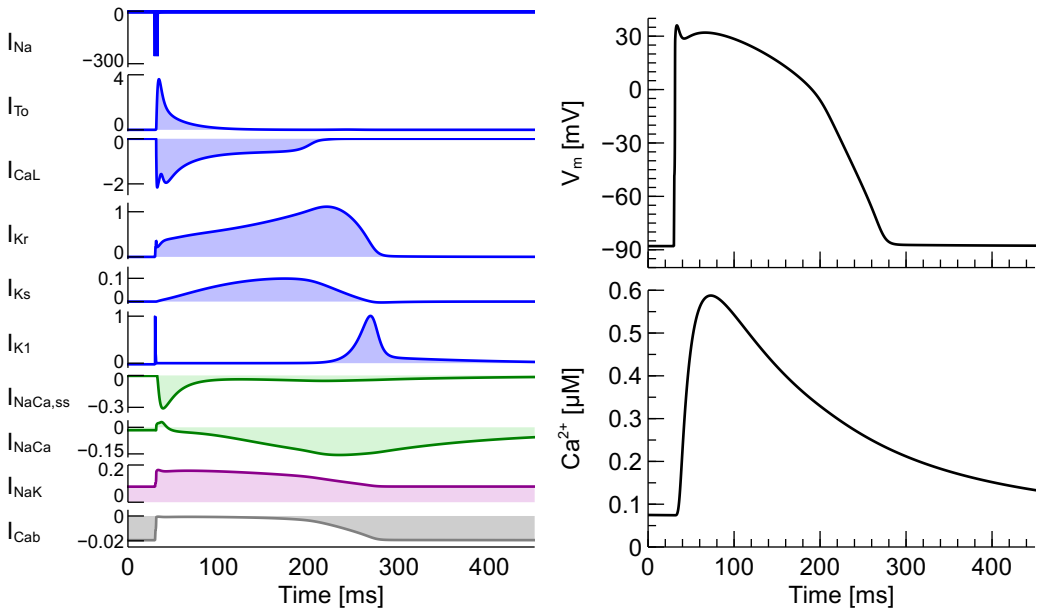


Figure 2.8: (Left) Currents through the cell membrane, simulated with the model by (O’Hara et al., 2011). For simplicity, some of the smaller currents are omitted. Note the wide variety of time-scales, shapes and amplitudes. (Right) The resulting action potential (top) and Ca^{2+} transient (bottom).

plateau phase, I_{Kr} grows steadily, while I_{CaL} begins to inactivate, eventually causing the membrane potential to drop. At around -50mV, the inward rectifier potassium current I_{K1} becomes active and brings V_m back down to the resting potential.

Once the cell is back at its resting potential (once it has *repolarized*, in electrophysiology lingo) the ion channel currents largely disappear. Instead, the membrane potential is determined by the balance of the sodium-potassium pump current I_{NaK} , the sodium-calcium exchange current I_{NaCa} and the sodium and calcium background currents, one of which (I_{Cab}) is shown Fig. 2.8. The current I_{K1} is also active in this phase, but as it has a reversal potential very close to the resting membrane potential, the current is typically small. However, if any minor deviations in V_m occur, they are immediately compensated by an increase in I_{K1} .

A final current visible in the figure is the slow delayed rectifier potassium current I_{Ks} . During a normal AP, it has a very low amplitude, and can be blocked entirely without apparent consequence. However, if an AP is prolonged excessively or if adrenaline is present (e.g., when something triggers the body’s ‘fight-or-flight’ response), I_{Ks} can grow to become a dominant force in restoring the resting potential (Volders et al., 2003). This is an example of redundancy in the cellular AP, an area where nature has introduced multiple mechanisms that appear to have the same function but can in fact act as back-up systems for each other. This is discussed further in Chapter ??.

2.8 Models of coupled cells and tissue

Once an AP model has been defined, it can be extended into a model of cardiac tissue. To create a model of two cells, the AP model's equations are duplicated, leading to two V_m 's, two sodium currents, two Ca^{2+} concentrations etc. A gap junction current is introduced to couple both cells:

$$\begin{aligned} I_{1 \rightarrow 2} &= g_{12} \cdot (V_1 - V_2) \\ I_{2 \rightarrow 1} &= g_{21} \cdot (V_2 - V_1) = -I_{1 \rightarrow 2} \end{aligned}$$

where $I_{1 \rightarrow 2}$ is the current from cell 1 to 2, $I_{2 \rightarrow 1}$ is the current from 2 to 1, V_1 and V_2 are the membrane potentials of cell 1 and 2 and $g_{12} = g_{21}$ is a fixed conductance indicating the strength of the connection. $I_{1 \rightarrow 2} = -I_{2 \rightarrow 1}$, indicating that this is a charge conserving connection. The exchange of ions between cells associated with this current is not commonly modeled. This scheme can be extended to any number of cells and allows arbitrarily complex networks of connections.

Modeling each cell individually, however, is not a particularly *fast* way of modeling tissue. This issue is solved in the *monodomain* model, which ignores the distinction between cells and uses AP models to describe *points in space*, connected by a resistance dictated by a continuous scalar field. Instead of the ordinary differential equations (ODEs) of single or coupled cell models, this results in partial differential equations (PDEs). The computational speed-up is achieved by solving the PDE on a grid with points spaced further apart than individual cell lengths (Leon and Horáček, 1991). The *bidomain* model is like the monodomain model, but has the additional benefit of incorporating extracellular conduction, which can be useful to model defibrillation (Keener and Sneyd, 2009). The relation between the monodomain model and the coupled cell approach is discussed in the appendix to Chapter ?? . For a detailed guide to large-scale tissue modeling, see Clayton and Panfilov (2008).

2.9 Conduction velocity and reentry

In systems of coupled cells, APs can propagate from cell-to-cell, causing waves of excitation to spread over the tissue. The speed at which they travel is called the *conduction velocity* (CV) and is an important tissue-level parameter. The CV is determined by the characteristics of the cardiac fast sodium current I_{Na} , the number of the gap junctions connecting the cells, and the presence of any fibrotic (non-conductive) material between cells. The number of gap junctions and the amount of fibrosis are both modeled by the cell-to-cell conductance terms specified by the tissue model. The influence of I_{Na} is an example where the tissue-level behavior depends on the properties of the individual cells. As a result, validating a cell model, or even a current model, also requires inspecting tissue-level behavior.

In normal cardiac conduction, waves propagate from one side of the ventricles (or atria) to the other and then die out. But under certain conditions *spiral waves* can occur that rotate around a fixed or moving locus, and can continue for extended periods of time (a detailed overview is given in [Kléber and Rudy, 2004](#)). This phenomenon is known as *reentry* and was described and analyzed as early as 1913 ([Mines, 1913](#)). Reentry severely disrupts the pumping function of the heart, and occurs in some of the most serious forms of arrhythmia. An example of a reentrant wave is shown in Chapter ??.

2.10 Bioelectricity on the body surface

The combined electrical action of all cardiomyocytes creates a signal strong enough to be measured at the body surface, using electrodes placed on the skin. The resulting signal is called the *electrocardiogram* or ECG and is one of the most important diagnostic tools in clinical cardiology. In Chapter ?? we exploit the fundamental relationship between the cellular AP and the ECG to improve the quality of heart-surface potential reconstructions based on body-surface measurements. To do this, we use a heuristic method based on the coupled-cell approach (see [Section 2.8](#)) to perform highly simplified ‘whole-heart’ simulations, which we compare to fine-grained simulations performed using the monodomain model.

2.11 A personal note

Occasionally, people have been surprised to hear of electricity as a central feature of the heart, of the biological applications of mathematical theory, or of the intrusion of computer scientists into the biomedical world (and vice versa!). This ‘crossing-borders’ aspect is one of the things that makes computational cardiac electrophysiology rewarding and fun. At the same time, its inter-disciplinary nature doesn’t always fit well with administrative or educational systems (not to mention the difficulty of explaining your job at dinner parties). Sometimes, whether due to nurture or nature, a certain cultural difference also seems to exist between holders of engineering and biomedical degrees.

And yet a brief glance at history shows that the interplay between these fields can be very fruitful indeed. For example, both Hodgkin and Huxley (see [Chapter 2](#)) had a strong background in physics; Huxley had even intended to graduate in this discipline before switching to physiology. During the war, both were involved in the development and application of radar ([Nobel Media, 1963a,b](#)). The papers that resulted in their 1963 “Nobel prize in physiology or medicine” (shared with John Eccles) not only describe physiology experiments but also provide the building plans for the electrical devices needed to perform them ([Hodgkin et al., 1952](#)). A second Nobel prize for physiology or medicine was awarded to Neher and Sakmann in 1991 for their invention of the single-channel recording technique. Again, this work was highly technical in nature, and again the authors wrote in the accompanying biography about their love of biology and physics and the difficulty of choosing one over the other when applying for university ([Nobel Media, 1991a,b](#)).

Leaving Nobel prizes aside, it is fascinating to see how quickly technological advancements have influenced biology. Sticking with mid-twentieth century examples, the electronic negative-feedback amplifier concept was developed in the 1930s ([Kline, 1993](#)), patented in 1937 ([Black, 1937](#)), and formed the electronic basis of the voltage-clamp in 1947 ([Huxley, 2002](#); [Cole, 1968](#)). When Hodgkin and Huxley performed their simulations in 1952, they used “a hand-operated calculating machine”, but by 1960 both Richard Fitzhugh and Denis Noble had simulated APs on an analog (Fitzhugh) and a digital (Noble⁵) computer ([Huxley, 2002](#); [Fitzhugh, 1960](#); [Noble, 1960](#)). Before computational models were introduced, Baltazar van der Pol and Jan van der Mark used a system of flashing Neon tubes to model the normal heartbeat, sinoatrial block, and the impossibility of creating extra systoles by stimulating during the heart’s refractory period. They published their findings with this electronic model in 1928 ([Van der Pol and Van der Mark, 1928](#)).

There are multiple conclusions we can draw from these examples, but the few I’d like to highlight are (1) there is a close and historical relationship between the mathematical sciences and biology, cardiac electrobiology in particular, (2) becoming proficient in more than one

⁵In fact, Noble used one of only *two* such devices available in the United Kingdom at the time.

subject should be encouraged at every level, and (3) investments in science can pay off in unexpected ways. These points may be relevant to those in charge of university structure, university curricula, and scientific funding.

References

- Armstrong, C.M., 2006. Na channel inactivation from open and closed states. *Proceedings of the National Academy of Sciences* 103, 17991–17996.
- Armstrong, C.M., Bezanilla, F., 1977. Inactivation of the sodium channel. II. Gating current experiments. *The Journal of General Physiology* 70, 567–590.
- Beeler, G.W., Reuter, H., 1977. Reconstruction of the action potential of ventricular myocardial fibres. *The Journal of Physiology* 268, 177–210.
- Bers, D., 2001. Excitation-contraction coupling and cardiac contractile force. volume 237. Springer Science & Business Media.
- Black, H.S., 1937. Wave translation system. US Patent 2,102,671.
- Carbonell-Pascual, B., Godoy, E., Ferrer, A., Romero, L., Ferrero, J.M., 2016. Comparison between Hodgkin–Huxley and Markov formulations of cardiac ion channels. *Journal of Theoretical Biology* 399, 92–102.
- Clancy, C.E., Rudy, Y., 1999. Linking a genetic defect to its cellular phenotype in a cardiac arrhythmia. *Nature* 400, 566–569.
- Clancy, C.E., Rudy, Y., 2002. Na⁺ channel mutation that causes both Brugada and long-QT syndrome phenotypes: a simulation study of mechanism. *Circulation* 105, 1208–1213.
- Clancy, C.E., Zhu, Z.I., Rudy, Y., 2007. Pharmacogenetics and anti-arrhythmic drug therapy: a theoretical investigation. *American Journal of Physiology – Heart and Circulatory Physiology* 292, H66–H75.
- Clayton, R., Panfilov, A., 2008. A guide to modelling cardiac electrical activity in anatomically detailed ventricles. *Progress in Biophysics and Molecular Biology* 96, 19–43.
- Cole, K.S., 1968. Membranes, ions, and impulses: a chapter of classical biophysics. Univ of California Press.
- Coraboef, E., Weidmann, S., 1949. Potentiel de repos et potentiels d’action du muscle cardiaque, mesures a l’aide d’électrodes intracellulaires. *Comptes Rendus Des Seances De La Societe De Biologie Et De Ses Filiales* 143, 1329–1331.
- Fitzhugh, R., 1960. Thresholds and plateaus in the Hodgkin-Huxley nerve equations. *The Journal of General Physiology* 43, 867–896.
- Gillespie, D.T., 1976. A general method for numerically simulating the stochastic time evolution of coupled chemical reactions. *Journal of Computational Physics* 22, 403–434.
- Graham, J., Gerard, R., 1946. Membrane potentials and excitation of impaled single muscle fibers. *Journal of Cellular and Comparative Physiology* 28, 99–117.

- Gros, D.B., Jongsma, H.J., 1996. Connexins in mammalian heart function. *Bioessays* 18, 719–730.
- Heijman, J., 2012. General discussion chapter, in: *Computational analysis of β -adrenergic stimulation and its effects on cardiac ventricular electrophysiology*. Ph.D. thesis. Maastricht University, pp. 201–222.
- Hille, B., 1970. Ionic channels in nerve membranes. *Progress in Biophysics and Molecular Biology* 21, 1–32.
- Hille, B., 2001. *Ion Channels of Excitable Membranes*. Sinauer Associates, Incorporated.
- Hodgkin, A., 1950. Conduction of the nervous impulse: some recent experiments. *British Medical Bulletin* 6, 322–325.
- Hodgkin, A.L., Huxley, A., Katz, B., 1952. Measurement of current-voltage relations in the membrane of the giant axon of Loligo. *The Journal of Physiology* 116, 424–448.
- Hodgkin, A.L., Huxley, A.F., 1952a. The components of membrane conductance in the giant axon of Loligo. *The Journal of Physiology* 116, 473–496.
- Hodgkin, A.L., Huxley, A.F., 1952b. Currents carried by sodium and potassium ions through the membrane of the giant axon of Loligo. *The Journal of Physiology* 116, 449–472.
- Hodgkin, A.L., Huxley, A.F., 1952c. The dual effect of membrane potential on sodium conductance in the giant axon of Loligo. *The Journal of Physiology* 116, 497–506.
- Hodgkin, A.L., Huxley, A.F., 1952d. A quantitative description of membrane current and its application to conduction and excitation in nerve. *The Journal of Physiology* 117, 500–544.
- Huxley, A., 2002. From overshoot to voltage clamp. *Trends in Neurosciences* 25, 553–558.
- Irvine, L.A., Saleet Jafri, M., Winslow, R.L., 1999. Cardiac sodium channel Markov model with temperature dependence and recovery from inactivation. *Biophysical Journal* 76, 1868–1885.
- Katz, B., Miledi, R., 1972. The statistical nature of the acetylcholine potential and its molecular components. *The Journal of Physiology* 224, 665–699.
- Keener, J., Sneyd, J., 2009. *Mathematical Physiology*. *Interdisciplinary Applied Mathematics: Mathematical Biology*, Springer.
- Kléber, A.G., Rudy, Y., 2004. Basic mechanisms of cardiac impulse propagation and associated arrhythmias. *Physiological Reviews* 84, 431–488.
- Kline, R., 1993. Harold Black and the negative-feedback amplifier. *Control Systems, IEEE* 13, 82–85.
- Leon, L.J., Horáček, B.M., 1991. Computer model of excitation and recovery in the anisotropic myocardium: I. Rectangular and cubic arrays of excitable elements. *Journal of Electrocardiology* 24, 1–15.
- Mines, G.R., 1913. On dynamic equilibrium in the heart. *The Journal of Physiology* 46, 349–383.
- Molleman, A., 2003. *Patch clamping: an introductory guide to patch clamp electrophysiology*. John Wiley & Sons.
- Neher, E., Sakmann, B., 1976. Single-channel currents recorded from membrane of denervated frog

- muscle fibres. *Nature* 260, 799–802.
- Nobel Media, 1963a. Alan L. Hodgkin - Biographical [internet]. www.nobelprize.org. Accessed: 2016-06-10.
- Nobel Media, 1963b. Andrew F. Huxley - Biographical [internet]. www.nobelprize.org. Accessed: 2016-06-10.
- Nobel Media, 1991a. Bert Sakmann - Biographical [internet]. www.nobelprize.org. Accessed: 2016-06-10.
- Nobel Media, 1991b. Erwin Neher - Biographical [internet]. www.nobelprize.org. Accessed: 2016-06-10.
- Noble, D., 1960. Cardiac action and pacemaker potentials based on the Hodgkin-Huxley equations. *Nature* 188, 495–497.
- Noble, D., 1962. A modification of the Hodgkin-Huxley equations applicable to Purkinje fibre action and pacemaker potentials. *The Journal of Physiology* 160, 317–352.
- Noble, D., Garny, A., Noble, P.J., 2012. How the Hodgkin-Huxley equations inspired the cardiac physiome project. *The Journal of Physiology* 590, 2613–2628.
- Noda, M., Ikeda, T., Suzuki, H., Takeshima, H., Takahashi, T., Kuno, M., Numa, S., 1986. Expression of functional sodium channels from cloned cDNA. *Nature* 322, 826–828.
- Noda, M., Shimizu, S., Tanabe, T., Takai, T., Kayano, T., Ikeda, T., Takahashi, H., Nakayama, H., Kanaoka, Y., Minamino, N., 1984. Primary structure of *Electrophorus electricus* sodium channel deduced from cDNA sequence. *Nature* 312, 121–127.
- O’Hara, T., Virág, L., Varró, A., Rudy, Y., 2011. Simulation of the undiseased human cardiac ventricular action potential: model formulation and experimental validation. *PLOS Computational Biology* 7, e1002061.
- Olivetti, G., Giordano, G., Corradi, D., Melissari, M., Lagrasta, C., Gambert, Anversa, P., 1995. Gender differences and aging: effects on the human heart. *Journal of the American College of Cardiology* 26, 1068–1079.
- Payandeh, J., Scheuer, T., Zheng, N., Catterall, W.A., 2011. The crystal structure of a voltage-gated sodium channel. *Nature* 475, 353–358.
- Van der Pol, B., Van der Mark, J., 1928. The heartbeat considered as a relaxation oscillation, and an electrical model of the heart. *The London, Edinburgh, and Dublin Philosophical Magazine and Journal of Science* 6, 763–775.
- Rudy, Y., Silva, J.R., 2006. Computational biology in the study of cardiac ion channels and cell electrophysiology. *Quarterly Reviews of Biophysics* , 57–116.
- Rush, S., Larsen, H., 1978. A practical algorithm for solving dynamic membrane equations. *IEEE Transactions on Biomedical Engineering* , 389–392.
- Schuetze, S.M., 1983. The discovery of the action potential. *Trends in Neurosciences* 6, 164–168.
- Seyfarth, E.A., 2006. Julius Bernstein (1839–1917): pioneer neurobiologist and biophysicist. *Bio-*

logical Cybernetics 94, 2–8.

Soeller, C., Cannell, M., 1999. Examination of the transverse tubular system in living cardiac rat myocytes by 2-photon microscopy and digital image-processing techniques. *Circulation Research* 84, 266–275.

Verkhatsky, A., Krishtal, O., Petersen, O.H., 2006. From Galvani to patch clamp: the development of electrophysiology. *Pflügers Archiv* 453, 233–247.

Volders, P.G., Sipido, K.R., Vos, M.A., Kulcsár, A., Verduyn, S.C., Wellens, H.J., 1998. Cellular basis of biventricular hypertrophy and arrhythmogenesis in dogs with chronic complete atrioventricular block and acquired torsade de pointes. *Circulation* 98, 1136–1147.

Volders, P.G., Stengl, M., van Opstal, J.M., Gerlach, U., Spätjens, R.L., Beekman, J.D., Sipido, K.R., Vos, M.A., 2003. Probing the contribution of IKs to canine ventricular repolarization key role for β -adrenergic receptor stimulation. *Circulation* 107, 2753–2760.

Welsh, A.J., Greco, E.F., Fenton, F.H., 2017. Dynamics of a human spiral wave. *Physics Today* 70, 78–79.